Using Monte Carlo ray tracing simulations to model the quantum harmonic oscillator modes observed in uranium nitride

J. Y. Y. Lin*
California Institute of Technology, Pasadena, California 91125, USA

A. A. Aczel, D. L. Abernathy, and S. E. Nagler
Quantum Condensed Matter Division, Oak Ridge National Laboratory, Oak Ridge, Tennessee 37831, USA

W. J. L. Buyers
Chalk River Laboratories, Canadian Neutron Beam Center, National Research Council, Chalk River, Ontario, Canada K0J 1P0

G. E. Granroth†
Neutron Data Analysis and Visualization Division, Oak Ridge National Laboratory, Oak Ridge, Tennessee 37831, USA
(Received 13 March 2014; published 7 April 2014)

Recently an extended series of equally spaced vibrational modes was observed in uranium nitride (UN) by performing neutron spectroscopy measurements using the ARCS and SEQUOIA time-of-flight chopper spectrometers [A. A. Aczel *et al.*, Nat. Commun. **3**, 1124 (2012)]. These modes are well described by three-dimensional isotropic quantum harmonic oscillator (QHO) behavior of the nitrogen atoms, but there are additional contributions to the scattering that complicate the measured response. In an effort to better characterize the observed neutron scattering spectrum of UN, we have performed Monte Carlo ray tracing simulations of the ARCS and SEQUOIA experiments with various sample kernels, accounting for nitrogen QHO scattering, contributions that arise from the acoustic portion of the partial phonon density of states, and multiple scattering. These simulations demonstrate that the U and N motions can be treated independently, and show that multiple scattering contributes an approximate Q-independent background to the spectrum at the oscillator mode positions. Temperature-dependent studies of the lowest few oscillator modes have also been made with SEQUOIA, and our simulations indicate that the T dependence of the scattering from these modes is strongly influenced by the uranium lattice.

DOI: 10.1103/PhysRevB.89.144302 PACS number(s): 61.05.F−, 63.20.dd

I. INTRODUCTION

Recent neutron scattering measurements of the vibrational response in uranium nitride (UN) revealed that the nitrogen atoms behave as nearly independent, ideal three-dimensional (3D) quantum harmonic oscillators (QHOs) [1] in this binary crystal. The quantum oscillations of the nitrogen atoms manifest themselves as a set of equally spaced, well-defined modes that can be measured to energies at least ten times as large as that of the fundamental $n = 1$, 50 meV mode. The intensity of these modes is well described by the expected response for a quantum harmonic oscillator in the $T = 0$ limit, with the intensity of the nth mode given by [2]

$$S_n(Q,\omega) = \frac{1}{n!}\left(\frac{\hbar Q^2}{2m\omega_o}\right)^n \exp\left(\frac{-\hbar Q^2}{2m\omega_o}\right)\delta(\hbar\omega - n\hbar\omega_o), \quad (1)$$

where ω_o is the fundamental frequency of the oscillator, $\exp(-\hbar Q^2/2m\omega_o)$ or $\exp(-2W)$ is the Debye-Waller factor, and m is the mass of the nitrogen atoms. The analysis reported in Ref. [1] is primarily based on Eq. (1), as all of the experimental data in that work was collected at $T = 5$ K.

The present study examines next-order effects beyond the simple QHO behavior. Since uranium nitride is a binary crystal, one additional source of scattering arises from the uranium partial phonon density of states (PDOS). Therefore, there are scattering processes other than oscillator single-scattering events that need to be taken into account in the experimental data. For example, one can also have acoustic phonon single-scattering processes or multiple-scattering events that create some combination of acoustic phonons and oscillator modes.

In this study, we clarify the origin of these background contributions. The multiple scattering described above arises from using the only readily available single crystal of uranium nitride, which was designed for studying the weak magnetic excitations [3], and is roughly a cube with a volume of 1 cm^3. While Eq. (1) represents the intensity expected for a single-scattering event, since the oscillator modes are evenly spaced, multiple-scattering events in any combination of elastic and inelastic scattering will also result in intensity at the positions of the oscillator modes. In fact, these multiple-scattering QHO processes were identified as the dominant source of background in the experimental data. To account for this contribution, a Q-independent constant B_n was added to Eq. (1) in Ref. [1]. However, this Q-independent assumption is an approximation that bears more thorough testing, which is accomplished in this work. Furthermore, other weaker background terms are modeled in this current study, including contributions that arise from the acoustic phonons.

*linjiao@caltech.edu
†granrothge@ornl.gov

The present work also investigates the effects of the finite uranium mass on the temperature dependence of the nitrogen QHOs. For these descriptions, a model that includes some T dependence is given by [2]

$$S_n(Q,\omega) = \exp(-2W) I_n(y) \exp\left(\frac{n\hbar\omega_o}{2k_B T}\right) \mathcal{F}(\omega). \qquad (2)$$

Here, $I_n(y)$ is a modified Bessel function of the first kind, $y = \hbar Q^2/[2m\omega_o \sinh(\hbar\omega_o/2k_B T)]$, and $\mathcal{F}(\omega)$ is the function that describes the width of the mode depending on the model used. For a QHO, $\mathcal{F}(\omega) = \delta(\hbar\omega - n\hbar\omega_o)$, and functions for other models will be discussed later.

Monte Carlo (MC) ray tracing is a powerful tool for understanding how complex sets of optical components interact. Modern neutron scattering instruments are assemblies of many optical devices and therefore are well described by this tool. Basically, probability packets are randomly generated at a virtual source component according to the emission characteristics of the physical properties of the real source. The probability of each packet is then changed according to its interaction with each component downstream of the source, and therefore relatively simple models of each component can be developed.

When these models are assembled together, they produce the same complex and integrated behavior as is observed in real instruments. For neutron scattering applications, the use of these simulations has generally been restricted to instrument design. However, with the availability of large parallel computing clusters and software packages tuned to MC ray tracing [4–6], it is now possible to carry out this type of simulation and provide detailed understanding of direct-geometry inelastic neutron scattering experiments. The neutron trajectories are modeled from the time that the neutrons are emitted from the moderator, through a sample, until they are finally captured by ^{3}He detector tubes. For neutron ray tracing through a sample, one can turn on and off various scattering mechanisms and thus determine how each contributes to the measured scattering intensity. Simulations were performed to compare to the data presented in Ref. [1], and they have been extended to more recent data from the SEQUOIA time-of-flight chopper spectrometer that characterized the temperature dependence of the UN oscillator modes from $T = 8$ to 300 K.

These simulations have been employed to verify that multiple scattering creates nearly Q-independent background at the oscillator mode positions. The simulations have also shown that the measured scattering for uranium nitride can be reproduced extremely well by including nitrogen oscillator and acoustic phonon single-scattering events (which includes both one-phonon and multiphonon scattering), and also multiple-scattering processes that create any combination of oscillator excitations and acoustic phonons. Finally, the modeling has revealed that the nitrogen vibrational response is well described by certain aspects of the modified version of the quantum harmonic oscillator known as the binary solid model [2]. This more complex model attempts to explain how the finite mass of the uranium atoms affects the lifetime of the nitrogen oscillators in the system.

II. EXPERIMENTAL CONDITIONS

All neutron scattering measurements reported here were collected using the ARCS [7] and SEQUOIA [8,9] direct-geometry time-of-flight chopper spectrometers at the Spallation Neutron Source of Oak Ridge National Laboratory. For all of the neutron scattering experiments, the UN single crystal was sealed in an ultrathin Al sample can [10] with He exchange gas in a closed-cycle He refrigerator. Further details of the first SEQUOIA and ARCS experiments, conducted only at $T = 5$ K, are reported in Ref. [1]. In this work, we have extended these earlier measurements to a series of different temperatures using SEQUOIA because the fine resolution provides better definition of the individual harmonic oscillator modes and thus a clearer observation of the T dependence. For these measurements, a Fermi chopper with a slit spacing of 0.5 mm and a radius of curvature of 1.53 m was spun at 600 Hz with $E_i = 700$ meV, yielding a full width at half maximum energy resolution of 1.3% of E_i at the elastic line. The T_0 chopper was spun at 180 Hz to ensure only 700 meV neutrons were incident on the sample and to block prompt neutrons from the proton pulse hitting the source target.

Data were accumulated by combining measurements taken with several different incident neutron directions in the $[H\,H\,L]$ plane, and additionally averaged over the Debye-Scherrer rings about the incident-beam direction. The results were normalized to account for variations of the detector response and solid angle coverage with a vanadium standard. This procedure enabled an accurate determination of the orientationally averaged scattering response.

III. SIMULATION DESCRIPTION

In order to gain a better understanding of the interplay of various contributing factors to the observed scattering intensity for uranium nitride, the MC ray tracing program MCViNE [4] developed in the DANSE [11] software development project (Distributed Data Analysis for Neutron Scattering Experiments) was used to simulate the experiments. All simulations in this work consist of four steps: (1) simulation of the neutron beam incident on the sample, which depends on the instrument of choice (ARCS or SEQUOIA) and the experimental settings, including the T_0 chopper frequency and the Fermi chopper choice, phase, and frequency; (2) simulation of neutron scattering by the "sample assembly"; (3) simulation of the detector intersection of neutron rays scattered from the sample, and generation of event-mode NeXus data files that are in the same format as the measurement data files, but include extra information of event probability; (4) reduction of the simulated NeXus file to $I(Q,E)$. The goal of this four-step simulation process is to reproduce the experiment by a simulation with the highest accuracy possible.

Step 1, the simulation of the incident beams on the sample for ARCS and SEQUOIA, was derived from the McStas [5] instrument definitions used in the design phase of the instruments [8,12,13]. The ARCS and SEQUOIA beam simulations were validated by comparison to instrument monitor data as well as detector data from experiments on vanadium and $C_4H_2I_2S$ [7,9]. In this work, 10^9 neutron events emitted from the moderator were included in all of the simulations, and

the neutrons at the sample position were saved and reused in step 2.

In step 2, the sample is modeled as an object with a geometric shape and a collection of scattering kernels. The MCViNE framework uses this information to compute the path of a neutron ray through the sample, pick a scattering kernel for scattering, compute the properties of the scattered neutron, and rescatter the neutrons repeatedly if the multiple-scattering option is turned on. More details of how the sample assembly is constructed and the multiple scattering is treated in the simulations are given in Secs. 1 and 2 of the Appendix. The UN sample is modeled as a cube with a 1 cm^3 volume and, depending on which case is examined below, contains one or more of the following scattering kernels: an incoherent elastic-scattering kernel, an incoherent acoustic one-phonon scattering kernel, an incoherent acoustic multiphonon scattering kernel, and incoherent nitrogen QHO kernels [based on Eq. (1) or Eq. (2) above] with or without broadening. The QHO kernels and acoustic phonon kernels are discussed further in Secs. 3 and 4, respectively, of the Appendix. The scattering power of various kernels is solely determined from corresponding cross sections [14] and dynamic structure factors. By the nature of the technique owing to Monte Carlo random sampling, the simulations incorporate all aspects of instrumental resolution, including the neutron energy distribution arising from the moderator, choppers, and detector pixels, as well as the Q resolution coming from the guides, sample, and detector pixels.

In step 3, each neutron scattered by the sample is processed by a detector-system component and an event is recorded in the NeXus file if it intercepts a detector tube. In ray tracing through a detector system, the detector tube in which the event is detected is located using a hierarchically described collection of detector tubes, while the exact location and time of flight are found by a MC selection. More detailed descriptions are presented in Sec. 5 of the Appendix.

In step 4, the NeXus data generated in step 3 are reduced using MANTID [15]. The only difference between the simulated and measured data is that the intensities in the simulations are computed as the sum of the probabilities of all packets arriving in the bin of interest, while those in the data are total event counts. Therefore, the analysis work flow is identical and uses the same code base for both the simulated and the measured data.

Finally, to ensure that steps 2–4 were being performed correctly, they were cross checked with an ideal $I(Q,E) = \delta(Q - Q_0, E - E_0)$ sample kernel.

IV. COMPARISONS BETWEEN SIMULATIONS AND THE DATA

A. Nearly constant QHO multiple scattering

The Monte Carlo simulations provide a unique way to calculate the scattering expected from the sample. Specifically, we can run a simulation where our sample assembly includes only single-scattering events or as many orders of multiple scattering as makes physical sense. Furthermore, only a single multiplicative factor is required to scale the simulated data for comparison to experimental data. Figure 1(a) shows the measured UN spectrum on ARCS for $E_i = 500$ meV, and

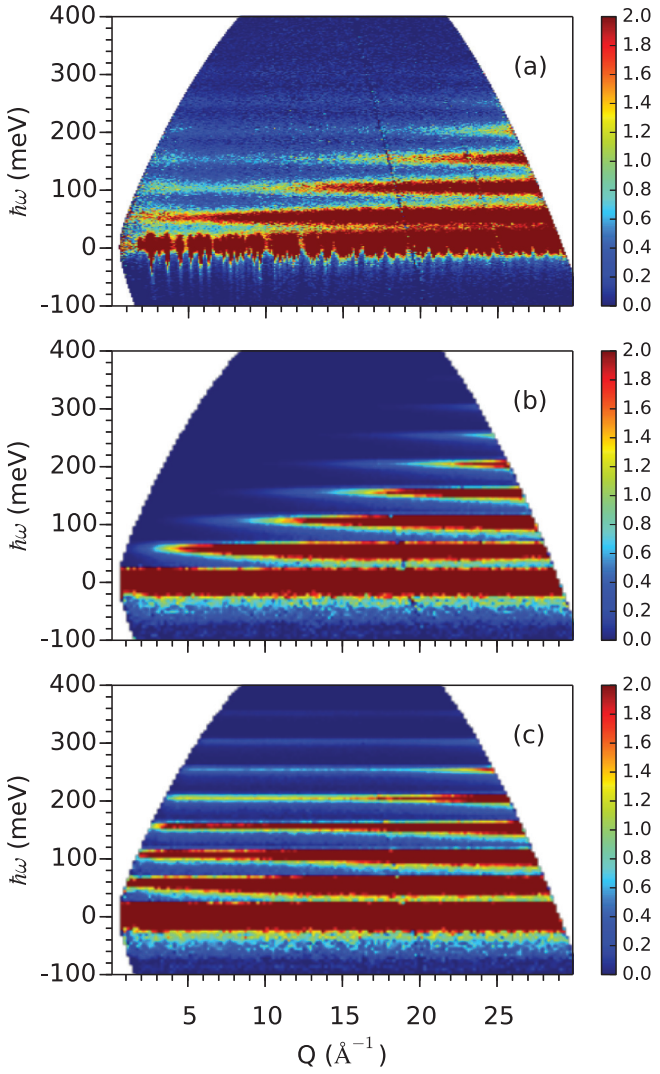

FIG. 1. (Color online) (a) Measured inelastic neutron scattering spectrum for UN from ARCS with $E_i = 500$ meV. (b),(c) Simulated inelastic neutron scattering spectrum for UN from ARCS with $E_i = 500$ meV. Only single-scattering QHO events are included in (b), while both single- and multiple-scattering QHO events are included in (c).

Fig. 1(b) shows the simulation for single QHO and elastic-scattering events corresponding to the same data set. As expected for the QHO model, there is no scattering for the higher-order modes at low Q. Figure 1(c) shows the QHO model with ten orders of multiple scattering included. The likelihood of the next order of multiple scattering decreases roughly according to a geometric progression from the present one (for more details, see Sec. 2 of the Appendix), so this limit should be sufficient and is consistent with the practice in other codes [16,17]. Notice that the simulation reveals how the low-Q portion of the modes arises from multiple scattering. For the lower-energy modes and the elastic line, the intensity is maximized at lower Q. Since the nitrogen oscillator modes are dispersionless and evenly spaced, it follows that any relatively high-energy mode composed of some combination of lower-energy modes and elastic events can produce more

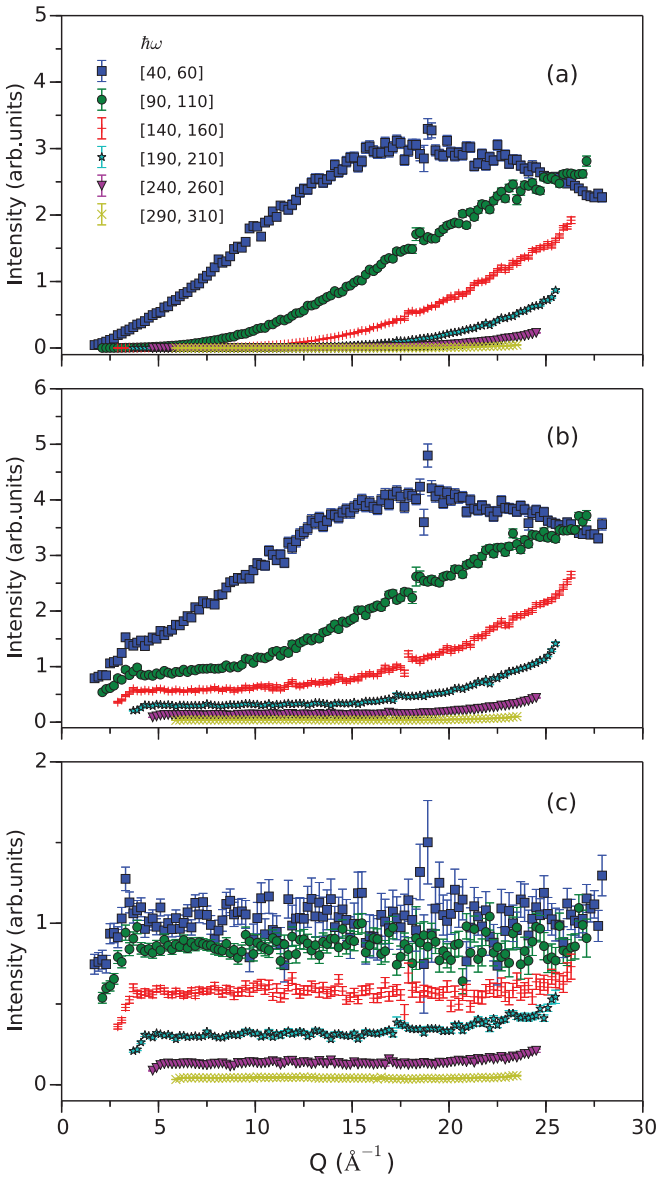

FIG. 2. (Color online) (a) A cut along Q for each mode from the simulation with no multiple scattering. (b) A cut along Q for each mode from the simulation with multiple scattering. (c) The difference between the curves in (a) and (b) which provides the multiple-scattering term in isolation from the QHO contribution. To a first approximation, this multiple-scattering term has no Q dependence, as was described in Ref. [1].

low-Q scattering at the mode positions than expected from single scattering only.

To quantitatively compare the intensity variations observed in Figs. 1(b) and 1(c) for each mode, a series of cuts were taken along Q with an energy width of 20 meV and centered about the different oscillator mode positions. The resulting cuts including single scattering only are shown in Fig. 2(a), and the case incorporating multiple scattering is shown in Fig. 2(b). To isolate the multiple-scattering contribution, the curves in Fig. 2(a) were subtracted from the curves in Fig. 2(b). The results are shown in Fig. 2(c). Over the Q range studied on ARCS and SEQUOIA, the simulation predicts a nearly Q-independent contribution arising from the multiple scattering at the oscillator mode positions. The simulation also shows that the intensity of the multiple scattering drops off rather quickly with increasing mode n. Both of these findings are in excellent agreement with experiment [1].

B. Effects of the acoustic phonons on the overall scattering

Figure 3(a) compares simulated and experimental ARCS $E_i = 500$ meV constant-E cuts centered at the oscillator mode positions, with the simulation including both single- and multiple-scattering elastic and QHO processes. The discrepancies between the observed and simulated $n = 1$ mode can be attributed to the fact that this simulation completely ignores the uranium atoms.

For a more accurate comparison, a another simulation was performed that included kernels in the sample assembly accounting for the scattering processes from the acoustic portion of the density of states. In our models, the acoustic motions of the lattice are decoupled from the QHO motions

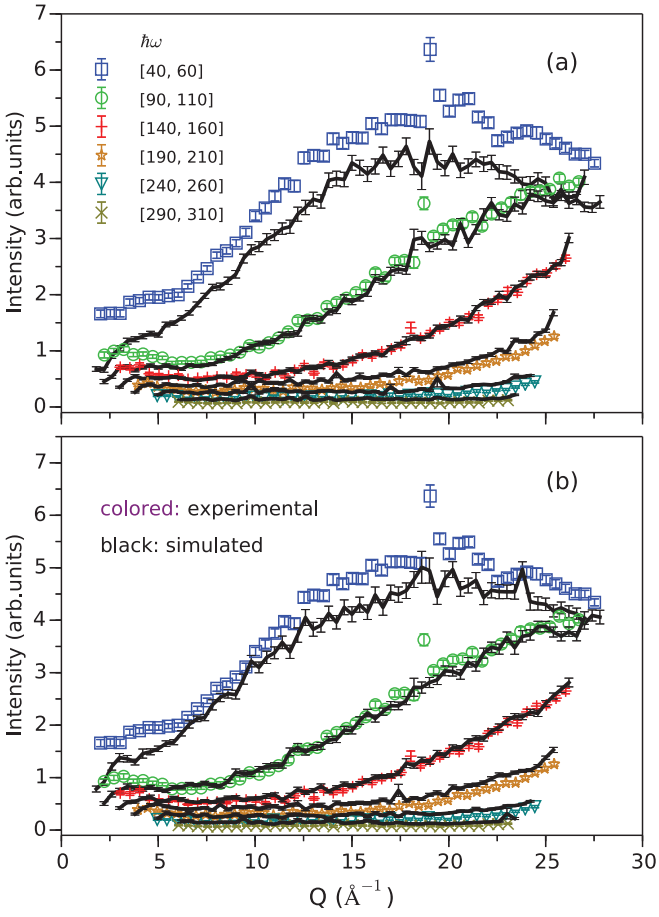

FIG. 3. (Color online) (a) Constant-E cuts. The black points are simulated using an elastic-scattering kernel and nitrogen QHO kernels, while the colored points are ARCS data with $E_i = 500$ meV. Note the excellent agreement for all modes except the $n = 1$ mode. (b) The same constant-E cuts, but the black points are now simulated using an elastic-scattering kernel, nitrogen QHO kernels, and acoustic phonon kernels. Note that the agreement for the $n = 1$ mode is much improved.

of the N. This is reasonable because of the large mass difference and is corroborated by density functional theory (DFT) calculations [18] of the partial density of states for each atom, which shows negligible influence on the acoustic modes by the N and similarly negligible influence on the optic or QHO modes by the U. As a result, we can work in the incoherent approximation [19–21], and simulate scattering from QHO modes and the acoustic modes independently. Multiple scattering was also turned on in this simulation, thereby including multiple-scattering processes up to the tenth order to account for various combinations of scattering from acoustic phonons, oscillator modes, and elastic processes. The result of this simulation is compared to experiment in the form of constant-E cuts, as shown in Fig. 3(b), and the agreement with experiment for the $n = 1$ mode in this case is much improved.

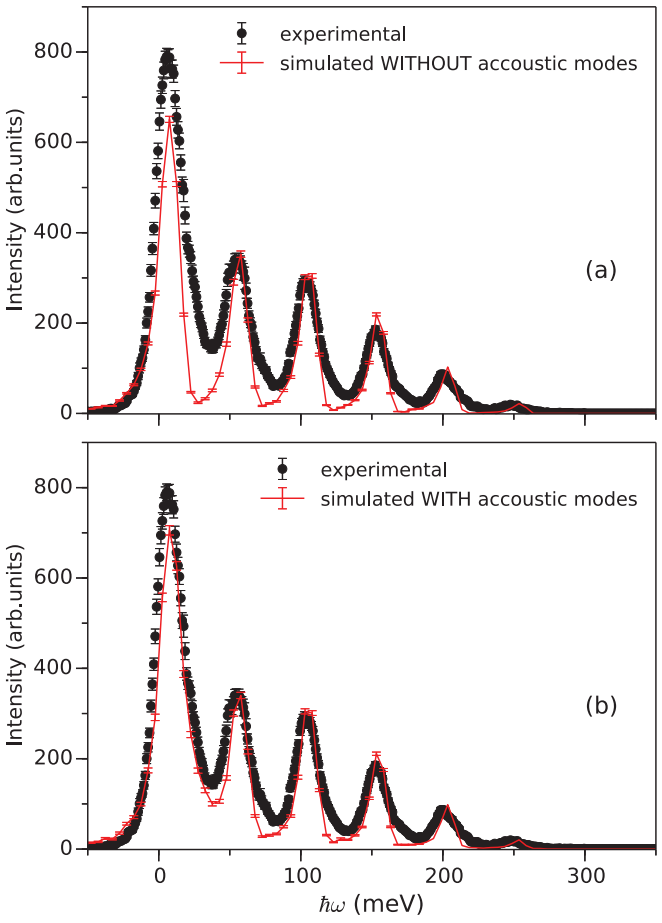

FIG. 4. (Color online) (a), (b) ARCS $E_i = 500$ meV data in black compared to simulated data in red, with an integration range of $Q =$ [24–26] Å^{-1} for both. In (a), the red curve was simulated using an elastic-scattering kernel and nitrogen QHO kernels. There is very good agreement between experiment and simulation, with the biggest discrepancies arising near the $n = 1$ and $n = 2$ modes. In (b), the red curve was simulated using an elastic-scattering kernel, nitrogen QHO kernels, and acoustic phonon density-of-states kernels. Note that the agreement in the low-energy regime, specifically around the $n = 1$ and $n = 2$ modes, is much improved.

Figure 4(a) compares simulated and experimental ARCS $E_i = 500$ meV data integrated over $Q = [24–26]$ Å^{-1}, with the simulation including only single- and multiple-scattering QHO processes. The largest discrepancies between the simulation and experiment are found at energies between the oscillator modes, with the most pronounced effects at low energies between the elastic line and the $n = 1$ mode, and between the $n = 1$ and $n = 2$ modes. Figure 4(b) shows how the situation improves when one includes the acoustic phonons in the simulation. The agreement between experiment and simulation in this case is quite remarkable, with only some small differences remaining in the energy ranges between the oscillator modes. The simulation even finds that the elastic peak position is not at zero-energy transfer, which is also consistent with the experimental data. This instrument-related feature is due to the asymmetric line shape that is produced in the moderator viewed by the instrument. The results presented in Figs. 3 and 4 clearly indicate that the overall response of uranium nitride can be modeled extremely well by incorporating nitrogen QHO scattering, the acoustic phonon density of states, and all forms of multiple scattering in the simulation.

C. Temperature dependence of the oscillator modes

The nitrogen atoms of UN are not completely isolated, but rather are embedded in a lattice of uranium atoms. Although the U atoms are very heavy, they still have a finite mass that can directly influence the QHO behavior of the nitrogen atoms. A simplified version of this situation, called the binary solid model, has been considered previously in Ref. [2]. The binary solid model applies to crystals composed of light and heavy atoms forming binary molecules, and explains how the motion of the heavy atoms affects the QHO behavior of the light ones. Although UN does not consist of binary molecules, this model or some modified version may be appropriate in this case.

The binary solid model makes definite predictions about the T dependence of the oscillator modes that should be readily measurable. To test these predictions, the temperature dependence of the nitrogen oscillator modes was investigated with SEQUOIA from $T = 8$ to 300 K. Figure 5 compares simulated and experimental $E_i = 700$ meV SEQUOIA data integrated over the full Q range for (a) $T = 8$ K and (b) $T = 300$ K. There are two different simulations for each temperature, with one corresponding to the simple QHO model and the other corresponding to the binary solid model. In the first case, the nitrogen atoms are modeled by Eq. (2) with $\mathcal{F}(\omega)$ representing the δ function. The acoustic phonon scattering and multiple-scattering contributions are also included in this simulation. In this case, the energy width of the oscillator modes arises only from the finite-energy resolution of the instrument. However, our data is not well described by this simple model at either temperature, and there is intrinsic broadening of the oscillator modes. This same broadening can also be seen in Fig. 4 when comparing the experimental data to the simulation, but it is less pronounced due to the coarser instrument resolution of ARCS.

In the second case, the sample assembly is modeled by a variant of the binary solid model [2], including the same scattering contributions associated with the acoustic portion

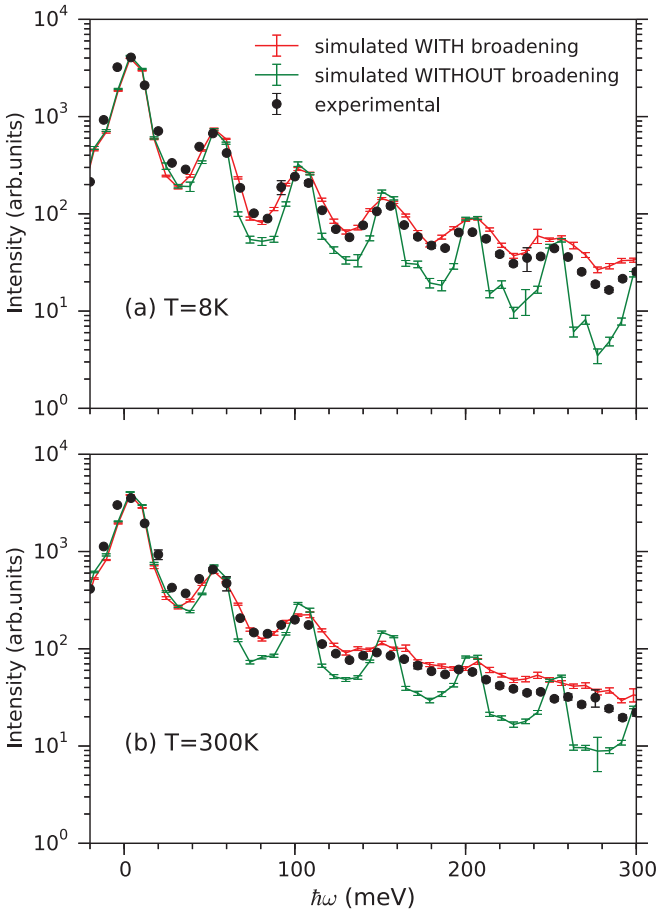

FIG. 5. (Color online) (a) $T = 8$ K, $E_i = 700$ meV, Q-integrated SEQUOIA data in black, compared to Q-integrated simulated data with and without intrinsic broadening, shown in red and green, respectively. The functional form of the intrinsic broadening is explained in the text. (b) The same three plots, but now for $T = 300$ K instead. The intrinsic broadening of the oscillator modes is well described by the binary solid model.

of the density of states and multiple scattering as before. The difference between the binary solid model and the simple QHO is that $\mathcal{F}$ is now given by

$$\mathcal{F} = \exp[-(\hbar\omega - n\hbar\omega_o)^2/2\Gamma^2(T)], \quad (3)$$

where the Gaussian width $\Gamma(T)$ is a function of temperature and given by

$$\Gamma^2(T) = (\hbar^2 Q^2/2M)\int_0^\theta du\, Z(u) u \coth(\hbar u/2k_B T). \quad (4)$$

In Eq. (4), $Z(u)$ is the acoustic phonon density of states (see Fig. 6), θ is the band maximum frequency for the acoustic phonon modes, and M is the mass of the uranium atoms.

The simulation including the QHO intrinsic broadening describes the SEQUOIA data very well at both temperatures, as shown in Fig. 5. This finding indicates that the intrinsic widths of the nitrogen oscillator modes are well described by the binary solid model, and therefore the finite lifetimes of these excitations can be attributed to their interactions with the uranium lattice.

The binary solid model also predicts that the oscillator modes will acquire dispersion with the form $\hbar\omega = n\hbar\omega_o + \hbar^2 Q^2/2M$. However, this dispersion was not observed in previous work [1] or in the data presented here, so we decided not to include this effect in our simulations. Although our experimental data is not consistent with all aspects of the binary solid model, we have shown that the uranium lattice plays an important role in governing the QHO physics in UN and any complete model needs to take the heavy U atoms into account.

V. CONCLUSIONS

We have used Monte Carlo ray tracing simulations with a variety of sample kernels to accurately model the total scattering response observed in a single crystal of uranium nitride on the SEQUOIA and ARCS time-of-flight chopper spectrometers. The simulations have verified that multiple scattering creates an essentially Q-independent background at the oscillator mode positions. The simulations have also shown that the measured scattering for uranium nitride can be reproduced extremely well by including QHO single-scattering events, acoustic phonon scattering events (both single and multiphonon), and multiple-scattering events that create any combination of oscillator excitations or acoustic phonons. Finally, the temperature dependence of the oscillator modes has been investigated on SEQUOIA from $T = 8$ to 300 K. Monte Carlo ray tracing simulations, incorporating intrinsic broadening of the oscillator modes according to the binary solid model, agree extremely well with the experimental data. This work shows that Monte Carlo ray tracing simulations can be an extremely effective tool for the accurate modeling of complex neutron scattering spectra.

ACKNOWLEDGMENTS

This research was supported by the U.S. Department of Energy, Office of Basic Energy Sciences. A.A.A., D.L.A., G.E.G., and S.E.N. were fully supported and J.Y.Y.L. was partially supported by the Scientific User Facilities Division. Neutron scattering experiments were performed at the Spallation Neutron Source, which is sponsored by the Scientific User Facilities Division. We thank B. Fultz, M. E. Hagen, A. I. Kolesnikov, A. J. Ramirez-Cuesta, G. D. Samolyuk, and G. M. Stocks for stimulating discussions. We also thank M. Reuter and S. Campbell for updating the MANTID code to read in the Monte Carlo generated data.

APPENDIX: SIMULATION TECHNIQUES

In this appendix, some details of the Monte Carlo simulations performed in this work are documented. In MCViNE, a neutron scatterer (for example, an aluminum rod, a vanadium plate, a single crystal sample and the furnace surrounding it, or a detector system) is modeled as a "composite neutron scatterer," which is a group of physical objects, each of which has its own shape and scattering properties. Scattering off a composite neutron scatterer happens by first investigating which of its constituents intersects the incident neutron ray, and then delegating to that particular constituent for scattering,

which could be composite itself and require another delegation for scattering. The hierarchical representation of neutron scatterers and this recursive algorithm work for both samples and detector systems, and can greatly improve computing efficiency.

A scatterer without constituent scatterers is termed an "elemental neutron scatter," and a common kind of elemental neutron scatterer is a "homogeneous scatterer," whose scattering function is homogeneous within its body. The scattering function of such scatterers is modeled as one scattering kernel or a combination of several scattering kernels, each of which represents one of the scattering mechanisms, such as incoherent one-phonon scattering or elastic coherent scattering.

In the following sections, a brief description of the sample assembly is given and how the multiple scattering is treated in the simulations is explained. Details of the various sample scattering kernels are also presented, and the simulation of the ARCS and SEQUOIA detector systems is explained in the last section.

1. Sample assembly

At the sample position, the hierarchical representation of neutron scatterers is termed the "sample assembly." A sample assembly specification includes geometrical shapes and positions/orientations of constituent neutron scatterers, and properties of their scattering kernels.

2. Multiple scattering

When multiple scattering is enabled, at each scattering event inside a homogeneous scatterer, one incident neutron is split for efficiency into two neutrons and their probabilities are adjusted accordingly. One neutron goes through the scatterer with its probability lowered by attenuation, while the other is scattered by one of the scattering kernels of the scatterer, chosen by a MC random selection, at a point also randomly selected along the forward path of the incident neutron. This splitting process repeats for the scattered neutron until either the neutron's weight is lower than a preselected limit or the maximum multiple-scattering order is reached. At this point, the neutron that is still inside the scatterer is allowed to propagate out, with its probability attenuated appropriately. The approach here is consistent with those in legacy programs [17].

3. QHO and binary solid model sample kernels

The sample kernels are used to simulate the scattering from the nitrogen atoms. In the simulation without intrinsic broadening, a series of "E_Q" kernels is used. Its implementation allows specification of an analytical function for the dynamic structure factor in the form of $S(Q,E) = S(Q)\delta[E - E(Q)]$. Note that this maps well onto Eq. (1), where for a QHO mode of order n, $E(Q) = n\hbar\omega_0$, and $S(Q)$ is defined by the prefactor in Eq. (1). Seven kernels corresponding to the seven lowest-order QHO modes make up the sample assembly for these simulations, whereas elastic scattering is simply included using the $n = 0$ term. All of these kernels use the N total scattering cross section.

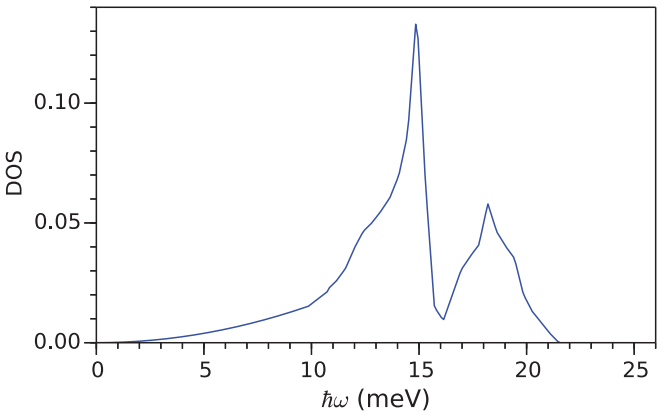

FIG. 6. (Color online) Uranium partial DOS.

To include the temperature broadening of the binary solid model, a series of "Broadened_E_Q" kernels is used, where $S(Q,E)$ is given by Eqs. (2)–(4) in the paper.

The QHO kernels were validated simply by comparing reduced $I(Q)$ curves to analytical expressions.

4. U phonon kernels

The U phonon kernels simulate neutron scattering from uranium phonons, using the incoherent approximation with the U total scattering cross section. In the incoherent approximation, both one-phonon and multiphonon scattering depends solely on the density of states (DOS) of the U phonons, which is computed by using a Born-Van Karmen (BvK) model derived from Ref. [22], and plotted in Fig. 6. Specifically, the U-U force constant 50 N/m and U-N force constant 65 N/m were used.

The incoherent elastic-scattering kernel is simply a nearly isotropic scattering kernel with a Debye-Waller factor. The incoherent one-phonon scattering kernel is implemented following Squires [20]:

$$S_{inc\pm1}(Q,\omega) = \frac{\hbar^2 Q^2}{2M}\exp(-2W)\frac{Z(E)}{E} \times \left\{\coth\left(\frac{1}{2}\beta E\right) \pm 1\right\}\Big/2. \quad \text{(A1)}$$

The multiphonon kernel is implemented following Ref. [23], Sec. 6.5: "Calculation of multiphonon scattering."

All phonon-related kernels were validated by comparing experimental measurements and simulations for vanadium and aluminum samples. The excellent agreement between the experimental data and the simulations for UN shows that the incoherent approximation works well to describe the scattering response from the orientationally averaged acoustic phonons.

5. Detector component

As mentioned earlier, a generic simulation scheme was designed for neutron scatterers that works for both sample assemblies and detector systems. The only specialization for detector systems involves scattering kernels of elemental detector components such as detector tubes. The scattering

kernel for a ^{3}He detector tube, for example, only absorbs neutrons. The hierarchical approach allows us to construct fairly sophisticated detector systems such as that of ARCS (3 rows of about 38 detector banks positioned and oriented roughly on a cylindrical surface; 117 760 pixels) and SEQUOIA (114 688 pixels) with ease.

Ray tracing of a neutron through a detector system happens in a multiscale way. When a neutron is sent to the ARCS detector system, for example, its intersection with the top scale composite scatterer with a "coarse-grained" hollow-cylinder-like shape is computed. If the intersection happens at that level, the search algorithm goes one level deeper in the detector system hierarchy to search for the detector component that intersects the neutron, and so on and so forth. At the last (smallest) scale, the path of a neutron through a detector tube is computed, and a MC sampling picks a point in the path for the neutron to be absorbed at that position, which is also used to compute the pixel identifier (ID). Additionally, the appropriate weighting multiplier for neutron probability and the time of flight (tof) are computed for the neutron to be recorded as a detector event. The probability, pixel ID, and the tof channel are then written to a NeXus file for reading in MANTID.

[1] A. A. Aczel, G. E. Granroth, G. J. MacDougall, W. J. L. Buyers, D. L. Abernathy, G. D. Samolyuk, G. M. Stocks, and S. E. Nagler, Nat. Commun. **3**, 1124 (2012).

[2] M. Warner, S. W. Lovesey, and J. Smith, Z. Phys. B **51**, 109 (1983).

[3] T. M. Holden, W. J. L. Buyers, E. C. Svensson, and G. H. Lander, Phys. Rev. B **30**, 114 (1984).

[4] J. Y. Y. Lin, M. A. Aivazis, and B. Fultz, http://docs.danse.us/MCViNE (unpublished).

[5] K. Lefmann and K. Nielsen, Neutron News **10**, 20 (1999).

[6] G. Zsigmond, K. Lieutenant, S. Manoshin, H. N. Bordallo, J. D. M. Champion, J. Peters, J. M. Carpenter, and F. Mezei, Nucl. Instrum. Methods Phys. Res. Sec. A: Accel. Spectrom. Detect. Assoc. Equip. **529**, 218 (2004).

[7] D. L. Abernathy, M. B. Stone, M. J. Loguillo, M. S. Lucas, O. Delaire, X. Tang, J. Y. Y. Lin, and B. Fultz, Rev. Sci. Instrum. **83**, 015114 (2012).

[8] G. E. Granroth, D. H. Vandergriff, and S. E. Nagler, Physica B **385-86**, 1104 (2006).

[9] G. E. Granroth, A. I. Kolesnikov, T. E. Sherline, J. P. Clancy, K. A. Ross, J. P. C. Ruff, B. D. Gaulin, and S. E. Nagler, J. Phys.: Conf. Ser. **251**, 012058 (2010).

[10] M. B. Stone, M. J. Loguillo, and D. L. Abernathy, Rev. Sci. Instrum. **82**, 055117 (2011).

[11] B. Fultz *et al.*, Danse, http://danse.us (unpublished).

[12] G. E. Granroth and D. L. Abernathy, in *Proceeding of the ICANS-XVI*, edited by G. Mank and H. Conrad (Forschungszentrum Jülich GmbH, Jülich, Germany, 2003).

[13] G. E. Granroth, M. Chen, J. A. Kohl, M. E. Hagen, and J. W. Cobb, J. Neutron Res. **15**, 91 (2007).

[14] V. F. Sears, Neutron News **3**, 26 (1992).

[15] J. Taylor, O. Arnold, J. Bilheaux, A. Buts, S. Campbell, M. Doucet, N. Draper, R. Fowler, M. Gigg, V. Lynch *et al.*, Bull. Am. Phys. Soc. **57**, W26.10 (2012).

[16] E. Farhi, V. Hugouvieux, M. R. Johnson, and W. Kob, J. Comput. Phys. **228**, 5251 (2009).

[17] J. R. D. Copley, P. Verkerk, A. A. Van Well, and H. Fredrikze, Comput. Phys. Commun. **40**, 337 (1986).

[18] Z.-G. Mei, M. Stan, and B. Pichler, J. Nucl. Mater. **440**, 63 (2013).

[19] S. W. Lovesey, *Theory of Neutron Scattering from Condensed Matter*, Vol. 1 (Clarendon, Oxford, 1984).

[20] G. L. Squires, *Introduction to the Theory of Thermal Neutron Scattering* (Cambridge University Press, Cambridge, 1978).

[21] P. C. H. Mitchell, *Vibrational Spectroscopy with Neutrons: With Applications in Chemistry, Biology, Materials Science and Catalysis* (World Scientific, Singapore, 2005).

[22] F. A. Wedgwood, J. Phys. C **7**, 3203 (1974).

[23] B. Fultz *et al.*, Experimental Inelastic Neutron Scattering, http://www.cacr.caltech.edu/projects/danse/doc/Inelastic_Book.pdf (unpublished).